Observation of the aerosol plume from the 2022 Hunga Tonga - Hunga Ha'apai eruption with SAGE III/ISS

Clair Duchamp[1], Felix Wrana[2,3], Bernard Legras[1], Pasquale Sellitto[4], Redha Belhadji[4], and Christian von Savigny[2,3]

[1]Laboratoire de Météorologie Dynamique (LMD-IPSL)
[2]Institute of Physics
[3]University of Greifswald
[4]Univ. Paris Est Créteil and Université de Paris, CNRS, Laboratoire Interuniversitaire des Systèmes Atmosphériques, Institut Pierre Simon Laplace, Créteil, France

June 25, 2023

Abstract

The Tonga eruption of 15 January 2022 has released a long-lived stratospheric plume of sulfate aerosols. More than 15 months after, we focus on the high quality data series of SAGE III/ISS to determine the mean radius and size distribution of the aerosols and their total mass. We show that the persisting aerosols – with a mode width of 1.25 and an effective radius of 0.4 μm – differ from the significantly smaller background aerosols and from those measured during other recent stratospheric eruptions. The sulfuric acid mass between 50°S and 30°N is estimated to be very stable in spite of considerable redistribution in latitude at a value of 0.66 Tg ± 0.1 Tg, corresponding to an initial sulfur dioxide emission of 0.44 Tg. Such properties are expected to induce a small negative aerosol radiative forcing, thus facilitating the persistence of a climate warming due to the volcanic water vapour.

Observation of the aerosol plume from the 2022 Hunga Tonga – Hunga Ha'apai eruption with SAGE III/ISS

Clair Duchamp[1], Felix Wrana[2], Bernard Legras[1], Pasquale Sellitto[3,4], Redha Belhadji[3], Christian von Savigny[2]

[1]Laboratoire de Météorologie Dynamique (LMD-IPSL), CNRS, Sorbonne Université, ENS-PSL, École Polytechnique, Paris, France
[2]Institute of Physics, University of Greifswald, Greifswald, Germany
[3]Univ. Paris Est Créteil and Université de Paris-Cité, CNRS, Laboratoire Interuniversitaire des Systèmes Atmosphériques (LISA-IPSL), Créteil, France
[4]Istituto Nazionale di Geofisica e Vulcanologia (INGV), Osservatorio Etneo (OE), Catania, Italy

Key Points:

- The extinction of the stratospheric plume of the 2022 Tonga eruption is well modeled by a unimodal distribution of sulfate particles.
- The effective radius of the aerosols is large with values close to 0.4 µm, and a mode width of 1.25, from March 2022 to April 2023.
- We estimate a total H_2SO_4 mass in stratospheric sulfate aerosols of about 0.66 Tg corresponding to 0.44 Tg of SO_2 at the source.

Corresponding author: Clair Duchamp, clair.duchamp@lmd.ipsl.fr

Abstract

The Tonga eruption of 15 January 2022 has released a long-lived stratospheric plume of sulfate aerosols. More than 15 months after, we focus on the high quality data series of SAGE III/ISS to determine the mean radius and size distribution of the aerosols and their total mass. We show that the peristing aerosols – with a mode width of 1.25 and an effective radius of 0.4 µm – differ from the significantly smaller background aerosols and from those measured during other recent stratospheric eruptions. The sulfuric acid mass between 50°S and 30°N is estimated to be very stable in spite of considerable redistribution in latitude at a value of 0.66 Tg ± 0.1 Tg, corresponding to an initial sulfur dioxide emission of 0.44 Tg. Such properties are expected to induce a small negative aerosol radiative forcing, thus facilitating the persistence of a climate warming due to the volcanic water vapour.

Plain Language Summary

We study the stratospheric aerosol plume produced by the Hunga Tonga–Hunga Ha'apai eruption on 15 January 2022 based on the high quality solar occultation measurements of the instrument SAGE III onboard the ISS. These data reveal that the aerosol sizes are about twice as large as after other documented volcanic eruptions and that the total mass of H_2SO_4 in the liquid droplets of sulfate in the stratosphere has been very stable from March 2022, when it started to be well homogeneized in longitude, to November 2022, when it started to decay. The total mass of 0.66 Tg of H_2SO_4 is in good agreement with the early estimates of a stratospheric emission of 0.4-0.5 Tg of SO_2. The implication is that the aerosol radiative impact will not mask the persisting warming effect of the water vapour injected in the stratosphere by the eruption.

1 Introduction

The phreato-magmatic eruption of the Hunga Tonga-Hunga Ha'apai (HTHH) started on 20 December 2021 and went through an explosive phase on 15 January 2022 which was comparable in Volcanic Explosivity Index with Pinatubo (Poli & Shapiro, 2022). The atmospheric plume was exceptional by reaching the mesosphere with a maximum height of 58 km and by injecting a considerable amount of water that saturated the stratosphere at least up to 35 km leaving a +10% increase of the stratospheric water vapour (Carr et al., 2022; Millán et al., 2022; Khaykin et al., 2022). The initial injection of water might have been much larger as the estimated amount of solid ejecta is close to 7 km^3 (O'Callaghan, 2022) but the water in excess above saturation condensed rapidly and precipitated entraining the ash that mostly disappeared from the stratosphere (Legras et al., 2022). As a matter of fact, besides a thin cloud detected at 35 km during a few days (Khaykin et al., 2022; Baron et al., 2023), no depolarizing aerosols have been detected in the stratosphere above 18 km in the aftermath of the eruption (Legras et al., 2022), indicating that ash did not play an important role. In contrast to water, the early estimates of the SO_2 injection at 0.4-0.5 Tg (Millán et al., 2022; Carn et al., 2022) were modest compared to the 20 Tg of Pinatubo (Guo et al., 2004) and even to the 1.5 Tg of Raikoke (de Leeuw et al., 2021). However, the moist environment induced a fast conversion to sulfate aerosols (SA) (Zhu et al., 2022) that were detected as non depolarizing, presumably spherical, particles and the conversion was basically complete by the end of January (Legras et al., 2022). It was suggested that the initial estimate could have missed a large amount of already converted SO_2 and estimates of up to 1.5 Tg have been speculated on (Sellitto et al., 2022; Legras et al., 2022). Several estimates of the average size of the aerosols and of their evolution ranging from 0.2 µm to 1 µm have been provided from satellite retrievals and in situ measurements (Kloss et al., 2022; Schoeberl et al., 2022; Taha et al., 2022; Legras et al., 2022; Khaykin et al., 2022; Baron et al., 2023). Such dispersion has considerable impact on the persistence of aerosols in the stratosphere and their radiative im-

pact (Zhu et al., 2022; Sellitto et al., 2022; Zhang et al., 2022). More than 15 months after the eruption, the goal of this work is to provide a well documented survey of the size and distribution of the aerosols, using minimal assumptions by taking advantage of the high quality measurements of SAGE III/ISS.

2 Data & Methods

2.1 SAGE III/ISS

The instrument Stratospheric Aerosol and Gas Experiment III (SAGE III), onboard the International Space Station (ISS), has been providing measurements of solar and lunar occultation since June 2017 (Cisewski et al., 2014). The instrument provides aerosol extinctions at 9 wavelengths from 384 nm to 1543 nm, the latter near-infrared channel being an addition with respect to SAGE II which significantly extends the spectral range. The data are provided in 0.5 km steps between 0 and 45 km altitude. The instrument observes about 15 sunrises and 15 sunsets per day with a latitudinal range which varies depending on the period of year (cf Table S1). In particular, there are no profiles at higher latitudes than 50°S between May and July 2022. The aerosol extinctions are retrieved as residuals of a spectral multilinear fit for O_3 and N_2O but do not require any size distribution assumptions unlike instruments with limb-scatter geometry like OMPS-LP (Loughman et al., 2018).

For this study, we use the version 5.3 of the SAGE III/ISS level 2 solar aerosol product. The profiles are monthly averaged in four latitude bands of width $\Delta\phi = 20°$, using data from November 2021 to April 2023. Due to its sparse geographical sampling, SAGE III began to see the HTHH SA plume only in March 2022 limiting our approach to the months after March 2022. During January and February 2022, SAGE III seldom sampled the plume and data are used for comparison between the plume and background conditions.

2.2 Retrieval of aerosol size parameters at 3 wavelengths

We use a method implemented by Wrana et al. (2021) to retrieve the SA size distribution which is based on the two color ratios 449 nm / 755 nm and 1543 nm / 755 nm for the aerosol extinction coefficients. These ratios are modeled for spherical liquid SA through Mie calculations using miepython, a python code where the Mie theory is implemented following the procedure described by Wiscombe (1979). We use fixed refractive indices from the GEISA spectroscopic database (Armante et al., 2016), for a temperature of 215 K and a H_2SO_4 weight proportion w_s of 70 % considering that the rest of the liquid droplet is water (Biermann et al., 2000). This weight proportion has been obtained according to Tabazadeh et al. (1997) using ambient temperature and moisture of the plume. As the SA have a very low absorption in the short wave spectral range (Palmer & Williams, 1975), we fix the imaginary part of the refractive index to 10^{-6}. Due to the presumed absence of ash, we assume that the particle size distribution (PSD) follows a monomodal lognormal distribution law.

$$\mathcal{N} = \frac{N_0}{\sqrt{2\pi} r \ln \sigma} \exp\left(-\frac{\ln^2 (r/r_m)}{2 \ln^2 \sigma}\right) \tag{1}$$

where σ is the mode width, r_m is the median radius and N_0 is the number density. The aerosol extinction k_{ext} at wavelength λ is then obtained by an integration over the size distribution

$$k_{ext}(\lambda) = \int_0^{+\infty} Q_{ext}(r, n, \lambda) \cdot \pi r^2 \cdot \mathcal{N}(r, r_m, \sigma, N_0)\, \mathrm{d}r \tag{2}$$

where Q_{ext} is the extinction efficiency factor from Mie calculations and n is the refractive index.

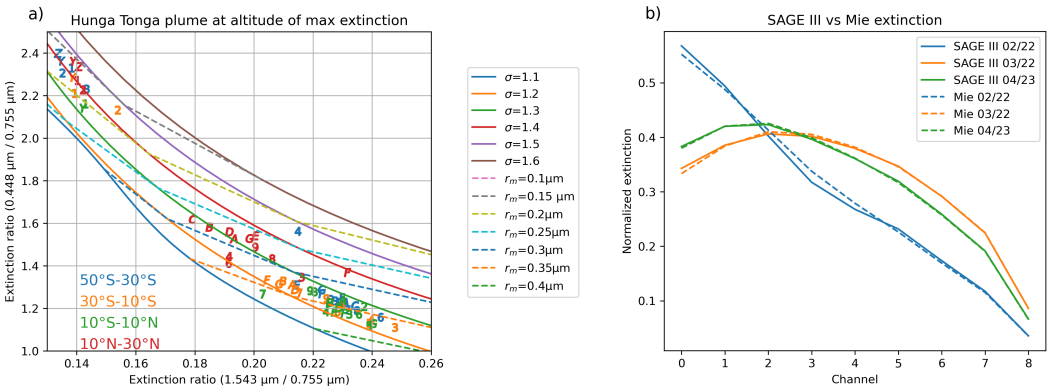

Figure 1. (a) The solid curves correspond to Mie calculations of the extinction ratios 448 nm / 755 nm and 1543 nm / 755 nm for constant values of the width σ. The dashed curves correspond to constant values of the mean radius r_m. This figure uses the same axis as Fig. 2a of Wrana et al. (2021). The numbers and letters show SAGE III measured ratios for each latitude band (color coded) and month at the central level of maximum 755 nm extinction for each month. The months are coded as Y and Z for November and December 2021, as 1 to 9 between January and September 2022 and alphabetically from A to G between October 2022 and April 2023. For each latitude band, the altitude levels for months before February 2022 (and March for the 40°S band) are chosen to be the same as the central level for the first detection in March 2022 (or April for the 40°S band). (b) Comparison of SAGE III (solid) and modeled (dash) normalized extinctions for all 9 aerosol channels of SAGE III. The curves are shown for the latitude band 30°S - 10°S using the values of σ and r_m determined from the diagram (a). We show the background case of February 2022 (blue) and the earliest and latest case of the plume in March 2022 (orange) and April 2023 (green).

In the estimation of the two extinction ratios mentioned above, the N_0 parameter cancels out, and we are left with a dependency on σ and r_m only. Fig. 1a shows that the curves for equal σ and r_m form a skewed grid in the domain of interest allowing the identification of the two parameters. The separation of spectral channels in terms of wavelengths in the two ratios is critical to obtain such results as shown by Wrana et al. (2021). For each data point from SAGE III extinctions the corresponding σ and r_m values are obtained by interpolating linearly between the discretized curves shown in Fig. 1a. Then, the particle effective radius r_{eff} can be estimated as $r_{eff} = r_m \exp\left(\frac{5}{2}\ln^2\sigma\right)$. Finally, we can compute the total number density N_0 from Eq. (2) using the extinction at 755 nm.

The good performance of the method can be appreciated from Fig. 1b where modeled Mie extinctions using σ and r_m drawn from Fig. 1a are compared to the SAGE III measured extinctions for three cases, one in the background and two in the plume at one-year distance. We see that the agreement is excellent over the whole range in spite of the obvious differences between the background and the plume cases. This is consistent with the absence of a coarser mode due to ash but does not rule out the presence of a finer mode which cannot be distinguished by extinction measurements (von Savigny & Hoffmann, 2020). The fact that estimates of sizes from fall speed (Schoeberl et al., 2022; Legras et al., 2022; Khaykin et al., 2022) using measurements by limb scatter or lidar backscatter are of the order or larger than our own estimate is an indication that such a fine mode is not important here as the lidar measurements in particular would be much more sensitive to it than solar occultation measurements (von Savigny & Hoffmann, 2020).

2.3 Estimation of the H_2SO_4 total mass

The H_2SO_4 mass is estimated for each vertical layer and latitude band from the estimated values of σ and r_m in this domain. The volume proportion of H_2SO_4 in a droplet is $\gamma(w_s) = (1 + \frac{\rho_s}{\rho_w}(\frac{1}{w_s} - 1))^{-1}$ where ρ_s is the density of pure H_2SO_4 and ρ_w is the water density, and the H_2SO_4 mass of the droplet is $m_p(r, w_s) = \frac{4}{3}\pi r^3 \gamma(w_s)\rho_s$.

Integrating over the lognormal distribution, we find that the H_2SO_4 mass contained in a layer centered at latitude ϕ is :

$$m_l = V_l(\phi) \cdot m_p(r_m, w_s) \cdot \alpha(\sigma) \cdot N_0 \tag{3}$$

where $\alpha(\sigma) = \exp(\frac{9}{2}\ln^2\sigma)$ is the lognormal volume ratio and $V_l(\phi) = 4\pi R^2 H \cos\phi \sin(\Delta\phi/2)$ is the volume of the layer with $R = 6371$ km and $H = 500$ m.

Summing m_l over all the layers of the plume, we calculate the total mass for each month and each latitude band for a given w_s. Unless otherwise specified, we use $w_s =$ 70 %.

3 Results

The first row of Fig. 2 shows that the aerosol plume has persisted as a distinguished layer in the stratosphere until April 2023, 15 months after the eruption. Until May 2022 the plume was mainly contained between 30°S and 10°N and then started to spread towards higher latitudes in the southern hemisphere. In spite of the detection of filaments at high latitudes (Mishra et al., 2022; Khaykin et al., 2022), there was little spread beyond the equatorial band in the northern hemisphere. The plume descended constantly until November 2022 but with a latitude dependent speed, in agreement with the Brewer-Dobson circulation, the descent being faster at high latitudes. Since November 2022, the maximum extinction altitude has been stalling at mid-latitudes and slightly rising in the equatorial band. It is noticeable that for all latitudes north of 30°S the aerosol layer does not disperse in altitude and keeps a fairly constant thickness.

In Fig. 1a, the observed extinction ratios at the level of maximum extinction in the plume are distributed over a domain of the diagram that clearly differs from the back-

ground points. These latter match the values reported in Wrana et al. (2021) with width σ of 1.4-1.5 and radius r_m of 0.15-0.2 µm. Instead, all the plume points south of 10°N but a couple of outliers lay between the 1.2 and 1.3 σ curves and cluster around $r_m \approx 0.35$ µm. This finding of low σ values is important, since usually very different assumptions are made, e.g. in satellite limb-scatter retrievals or in size retrievals using a 2 wavelength-extinction-ratio approach, which can introduce strong retrieval biases. The part of the plume in the 10°N - 30°N range forms a separate cluster with smaller radius between 0.25 and 0.30 µm and $\sigma \approx 1.3$. April 2022 for the 40°S latitude band is a mixed case between background and plume conditions when aerosols begin to reach these latitudes (as seen on Fig. 2, first row). Fig. S1 shows that retrieval uncertainties do not jeopardize the separation between the background and the plume. It also shows that at all latitudes the mean size decreases with time albeit by a small amount but no trend can be detected for the width. From σ and r_m, we calculate r_{eff} which is near 0.4 µm in the plume while we find 0.2 µm or less for the background in agreement with Khaykin et al. (2022).

The full temporal evolution of σ and r_{eff} is shown in the second and third rows of Fig. 2. The homogeneity and the persistence of the properties across the plume and in time are clearly visible. Using the same method, Wrana et al. (2023) found σ values for other stratospheric volcanic plumes produced by the eruptions of Ambae in 2018, Raikoke and Ulawun in 2019 and La Soufrière in 2021, which are all larger, approaching respectively 1.5-1.6 and 1.8-2.0 (Wrana et al., 2023), reinforcing the exceptional aspect of the HTHH eruption.

The total number density N_0 is shown in the last row of Fig. 2. The largest values of about 5 cm^{-3} are found in the early stage of the equatorial band. Values of 3.5 cm^{-3} are maintained until September 2022 and are slowly declining afterwards.

Fig. 3 shows 2 retrieved PSD in the same latitude band and altitude range for the background conditions and the plume. We stress that the HTHH eruption actually led to a much wider size distribution than in the background, even though the mode width σ is strongly reduced. This is because σ is the distribution width in logarithmic radius space, not linear radius space.

Fig. 4a shows the total amount of H_2SO_4 mass in the plume SA and the background mass contribution in the volume of the plume, according to Eq. (3) for a value of the mass proportion w_s of 70%. The total amount between 50°S and 30°N remains remarkably constant from March 2022 to November 2022 in spite of a considerable redistribution in latitude which is shown in Fig. 4b. The fast transport to the equatorial band during the first month following the eruption mentioned by Schoeberl et al. (2023) generates an equatorial dominance until May 2022 which is followed by a transport to the 40°S band which dominates from August to November 2022. The total mass decline after November 2022 is mainly due to this latitude band, presumably because of the sedimentation towards the lowest stratosphere and return to the troposphere. The equatorial band and the 20°S band essentially exchange aerosol mass while maintaining a constant sum from August 2022 onward. Taking into account the high latitude contribution in the southern hemisphere, which can only be estimated from October 2022, adds 0.1 Tg to the total but does not contribute to the decline. If a distribution of sulfate representing a background component (to be substracted) is taken into account within the volume of the plume (see Fig. 4a), this represents a small correction which increases with the volume of the plume but is always less than 0.1 Tg. Accounting these errors, we estimate the total mass of H_2SO_4 between March and November 2022 to be 0.66 Tg ± 0.1 Tg for $w_s = 70\%$. It scales proportionally to w_s if another value is assumed.

Converting the H_2SO_4 total mass into a SO_2 source using the molar mass ratio produces an estimate of 0.44 Tg of SO_2 for 0.66 Tg of H_2SO_4 which is in good agreement with the early estimates (Millán et al., 2022; Carn et al., 2022) produced from satellite observations.

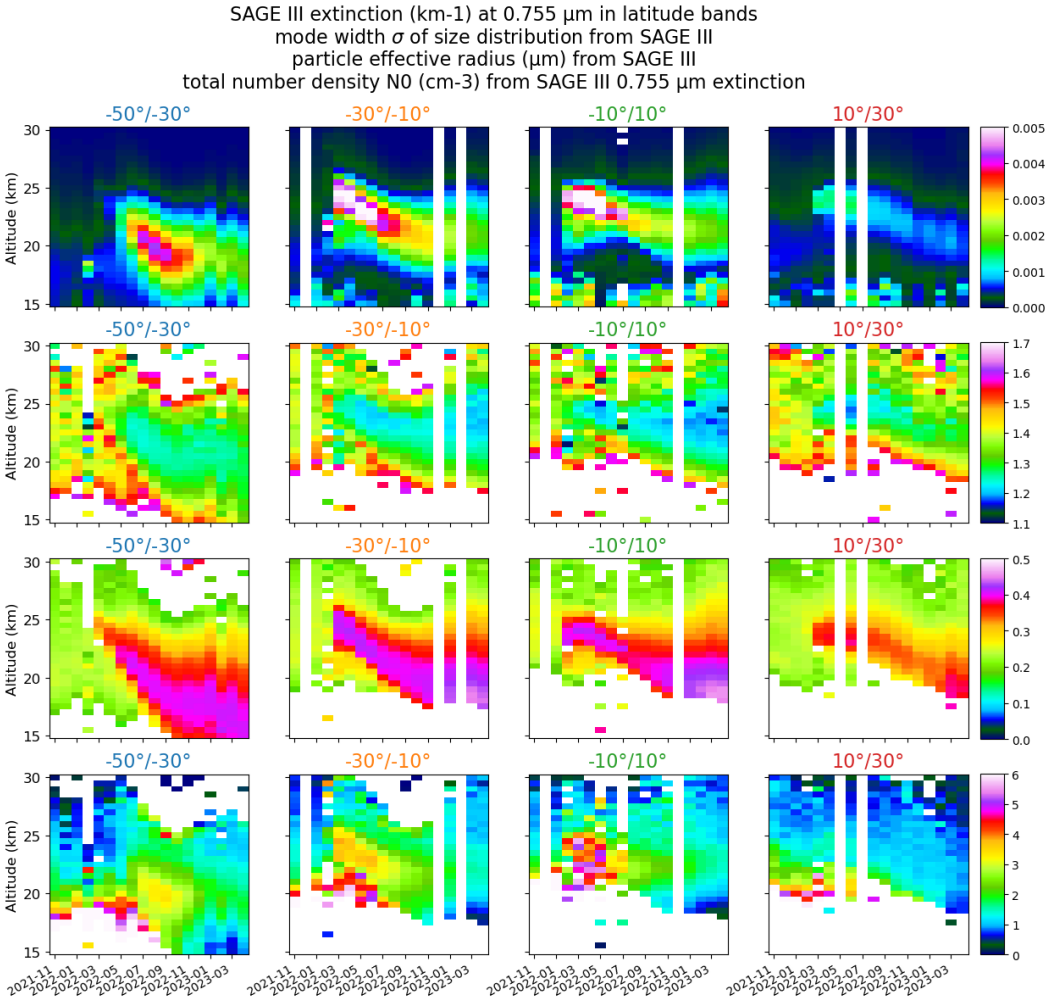

Figure 2. Zonal altitude-time sections averaged over 20° latitude bands between 50°S and 30°N. The first row represents the aerosol extinction k_{ext} (km^{-1}) provided by SAGE III at 755 nm. The second row represents the mode width σ of the PSD retrieved from SAGE III extinction ratios. The third row represents the particle effective radius r_{eff} (µm). The fourth row represents the total number density N_0 (cm^{-3}) of the PSD retrieved from SAGE III extinction ratios and 755 nm extinction k_{ext}.

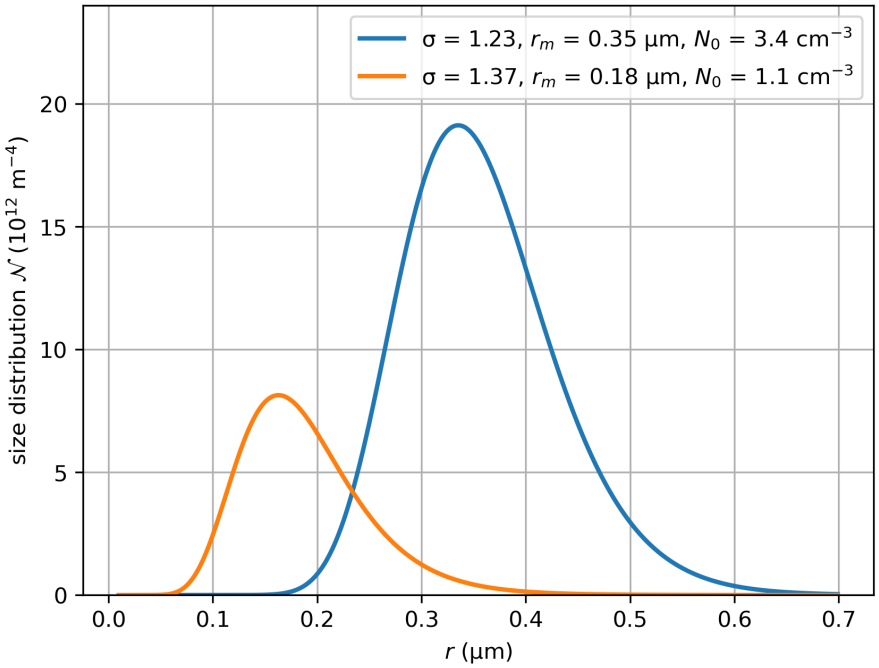

Figure 3. Monthly averaged particle size distributions from the retrieved PSD parameters in the 30°S - 10°S latitude range. Orange curve corresponds to background conditions at 24.5 km averaged between months of November 2021 and January 2022, blue curve corresponds to plume conditions at altitude of maximum extinction averaged between months of June and August 2022.

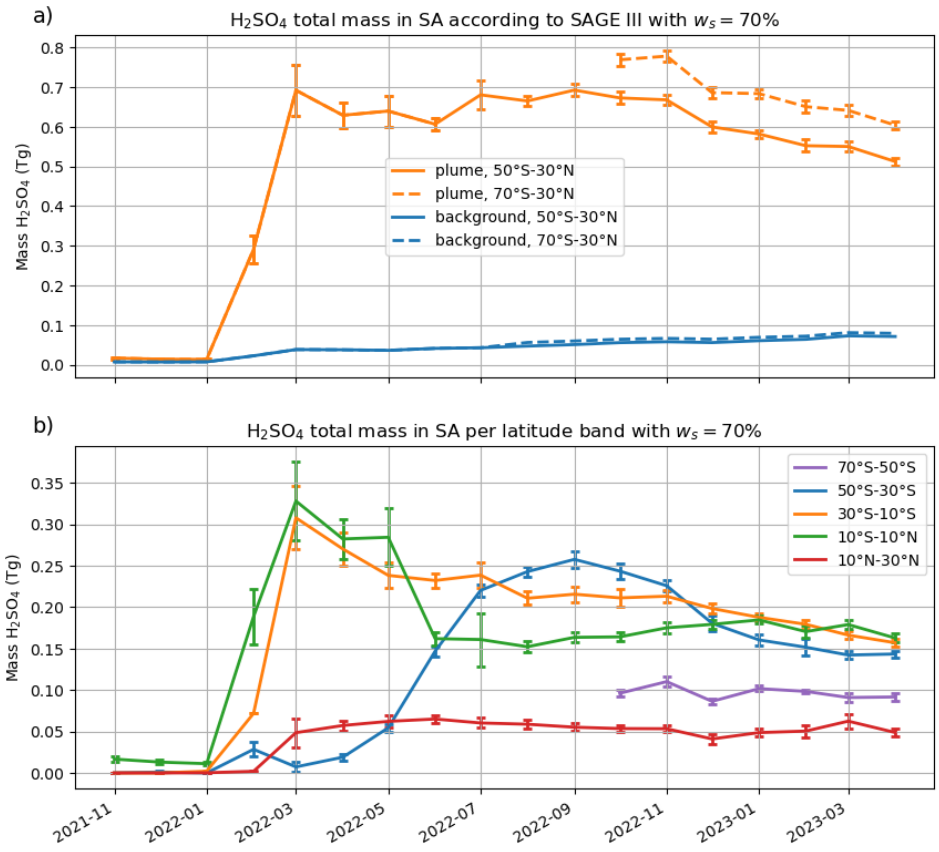

Figure 4. (a) Orange curves: evolution of the H_2SO_4 total mass contained in the plume sulfates for a H_2SO_4 weight percentage $w_s = 70\%$, according to SAGE III, eliminating surrounding pixels with radius r_m less than 0.2 µm considered as background. Blue curves: background contribution within the volume of the plume with $\sigma = 1.4$, $r_m = 0.15$ µm and $N_0 = 1$ cm^{-3}. The latitude range is 50°S - 30°N for solid curves and 70°S - 30°N for dashed curves. (b) Evolution of the H_2SO_4 total mass per latitude band. The contribution from the 50°S - 70°S is zero before May 2022, then is missing until August and contaminated by polar stratospheric clouds until September. It is shown only from October.

4 Conclusions

The HTHH eruption led to a large perturbation in stratospheric aerosols still visible 15 months after the eruption in solar occultation measurements of the satellite instrument SAGE III/ISS. The comparison of these measurements with theoretical Mie calculations supports the hypothesis of the absence of any optical signature of ash. Assuming a monomodal size distribution of liquid spherical sulfate aerosols, we estimate the mode width and the effective radius to the unusual values of $\sigma \approx 1.25$ and $r_{eff} \approx 0.4\,\mu m$ which have persisted at the plume peak height over 15 months with only a small decreasing trend in the size. The additional estimate of the total number density leads to an estimate of the total mass of stratospheric H_2SO_4 which is near 0.66 Tg for a mass proportion of 70% and has been found to be very stable over the period March 2022 to November 2022 after which it slowly declines. This mass matches very well previous estimates of the stratospheric SO_2 source of about 0.4-0.5 Tg (Millán et al., 2022; Carn et al., 2022).

The unusual size distribution of aerosols is related to the fast conversion of SO_2 to sulfates and possible sustained condensation/coagulation under very moist conditions documented by, e.g., Legras et al. (2022) and modeled by Zhu et al. (2022). Larger particles than recent stratospheric volcanic eruptions, like Raikoke and others, can be associated with a smaller aerosol radiative impact (Lacis et al., 1992). In the case of the extremely water-vapor-rich Hunga Tonga plume, this, in turns, facilitate the persistence of a global warming volcanic plume, as discussed by Sellitto et al. (2022).

Open Research Section

SAGE III/ISS L2 Solar Event Species Profiles (HDF5) V053 dataset is available from `https://doi.org/10.5067/ISS/SAGEIII/SOLAR_NetCDF4_L2-V5.3`. miepython is a free package available from `https://miepython.readthedocs.io/en/latest/` and `https://doi.org/10.5281/zenodo.8023972`. We used version 2.3.0 in this study. AERIS has provided access to the GEISA database at `https://geisa.aeris-data.fr`.

Acknowledgments

This study has been supported by the Agence Nationale de la Recherche under grant 21-CE01-0007-01 (ANR ASTuS) and the Centre National d'Études Spatiales (CNES). Work at the University of Greifswald was funded by the Deutsche Forschungsgemeinschaft (DFG Research Unit VolImpact, grant number 398006378).

References

Armante, R., Scott, N., Crevoisier, C., Capelle, V., Crepeau, L., Jacquinet, N., & Chédin, A. (2016, September). Evaluation of spectroscopic databases through radiative transfer simulations compared to observations. Application to the validation of GEISA 2015 with IASI and TCCON. *Journal of Molecular Spectroscopy*, *327*, 180–192. doi: 10.1016/j.jms.2016.04.004

Baron, A., Chazette, P., Khaykin, S., Payen, G., Marquestaut, N., Bègue, N., & Duflot, V. (2023). Early Evolution of the Stratospheric Aerosol Plume Following the 2022 Hunga Tonga-Hunga Ha'apai Eruption: Lidar Observations From Reunion (21°S, 55°E). *Geophysical Research Letters*, *50*(10), e2022GL101751. doi: /10.1029/2022GL101751

Biermann, U. M., Luo, B. P., & Peter, T. (2000). Absorption Spectra and Optical Constants of Binary and Ternary Solutions of H2SO4, HNO3, and H2O in the Mid Infrared at Atmospheric Temperatures. *The Journal of Physical Chemistry A*, *104*(4), 783-793. doi: 10.1021/jp992349i

Carn, S. A., Krotkov, N. A., Fisher, B. L., & Li, C. (2022). Out of the blue: Vol-

canic SO2 emissions during the 2021–2022 eruptions of Hunga Tonga—Hunga Ha'apai (Tonga). *Frontiers in Earth Science*, *10*, 976962. doi: 10.3389/feart.2022.976962

Carr, J. L., Horvath, A., Wu, D. L., & Friberg, M. D. (2022). Stereo Plume Height and Motion Retrievals for the Record-Setting Hunga Tonga-Hunga Ha'apai Eruption of 15 January 2022. *Geophysical Research Letters*, *49*, e2022GL098131. doi: 10.1029/2022GL098131

Cisewski, M., Zawodny, J., Gasbarre, J., Eckman, R., Topiwala, N., Rodriguez-Alvarez, O., ... Hall, S. (2014). The Stratospheric Aerosol and Gas Experiment (SAGE III) on the International Space Station (ISS) Mission. In R. Meynart, S. P. Neeck, & H. Shimoda (Eds.), *Sensors, systems, and next-generation satellites xviii* (Vol. 9241, p. 924107). SPIE. doi: 10.1117/12.2073131

de Leeuw, J., Schmidt, A., Witham, C. S., Theys, N., Taylor, I. A., Grainger, R. G., ... Kristiansen, N. I. (2021). The 2019 Raikoke volcanic eruption – Part 1: Dispersion model simulations and satellite retrievals of volcanic sulfur dioxide. *Atmospheric Chemistry and Physics*, *21*(14), 10851–10879. doi: 10.5194/acp-21-10851-2021

Guo, S., Bluth, G. J. S., Rose, W. I., Watson, I. M., & Prata, A. J. (2004). Re-evaluation of SO2 release of the 15 June 1991 Pinatubo eruption using ultraviolet and infrared satellite sensors. *Geochemistry, Geophysics, Geosystems*, *5*(4). doi: 10.1029/2003GC000654

Khaykin, S., Podglajen, A., Ploeger, F., Grooß, J.-U., Tence, F., Bekki, S., ... Ravetta, F. (2022). Global perturbation of stratospheric water and aerosol burden by Hunga eruption. *Communications Earth & Environment*, *3*(1), 316. doi: 10.1038/s43247-022-00652-x

Kloss, C., Sellitto, P., Renard, J.-B., Baron, A., Bègue, N., Legras, B., ... Jégou, F. (2022). Aerosol Characterization of the Stratospheric Plume From the Volcanic Eruption at Hunga Tonga 15 January 2022. *Geophysical Research Letters*, *49*(16), e2022GL099394. doi: 10.1029/2022GL099394

Lacis, A., Hansen, J., & Sato, M. (1992). Climate forcing by stratospheric aerosols. *Geophysical Research Letters*, *19*(15), 1607-1610. doi: 10.1029/92GL01620

Legras, B., Duchamp, C., Sellitto, P., Podglajen, A., Carboni, E., Siddans, R., ... Ploeger, F. (2022). The evolution and dynamics of the Hunga Tonga–Hunga Ha'apai sulfate aerosol plume in the stratosphere. *Atmospheric Chemistry and Physics*, *22*(22), 14957–14970. doi: 10.5194/acp-22-14957-2022

Loughman, R., Bhartia, P. K., Chen, Z., Xu, P., Nyaku, E., & Taha, G. (2018). The Ozone Mapping and Profiler Suite (OMPS) Limb Profiler (LP) Version 1 aerosol extinction retrieval algorithm: theoretical basis. *Atmospheric Measurement Techniques*, *11*(5), 2633–2651. doi: 10.5194/amt-11-2633-2018

Millán, L., Santee, M. L., Lambert, A., Livesey, N. J., Werner, F., Schwartz, M. J., ... Froidevaux, L. (2022). The Hunga Tonga-Hunga Ha'apai Hydration of the Stratosphere. *Geophysical Research Letters*, *49*(13), e2022GL099381. doi: 10.1029/2022GL099381

Mishra, M. K., Hoffmann, L., & Thapliyal, P. K. (2022). Investigations on the Global Spread of the Hunga Tonga-Hunga Ha'apai Volcanic Eruption Using Space-Based Observations and Lagrangian Transport Simulations. *Atmosphere*, *13*(12), 2055. doi: 10.3390/atmos13122055

O'Callaghan, J. (2022). Burst of underwater explosions powered Tonga volcano eruption. *Nature*, d41586–022–01544–y. doi: 10.1038/d41586-022-01544-y

Palmer, K. F., & Williams, D. (1975). Optical constants of sulfuric acid; application to the clouds of Venus? *Applied Optics*, *14*(1), 208–219. doi: 10.1364/AO.14.000208

Poli, P., & Shapiro, N. M. (2022). Rapid Characterization of Large Volcanic Eruptions: Measuring the Impulse of the Hunga Tonga Ha'apai Explosion From Teleseismic Waves. *Geophysical Research Letters*, *49*(8), e2022GL098123. doi:

10.1029/2022GL098123

Schoeberl, M. R., Wang, Y., Ueyama, R., Taha, G., Jensen, E., & Yu, W. (2022). Analysis and Impact of the Hunga Tonga-Hunga Ha'apai Stratospheric Water Vapor Plume. *Geophysical Research Letters*, *49*(20), e2022GL100248. doi: doi.org/10.1029/2022GL100248

Schoeberl, M. R., Wang, Y., Ueyama, R., Taha, G., & Yu, W. (2023). The Cross Equatorial Transport of the Hunga Tonga-Hunga Ha'apai Eruption Plume. *Geophysical Research Letters*, *50*(4), e2022GL102443. doi: 10.1029/2022GL102443

Sellitto, P., Podglajen, A., Belhadji, R., Boichu, M., Carboni, E., Cuesta, J., ... Legras, B. (2022). The unexpected radiative impact of the Hunga Tonga eruption of 15th January 2022. *Communications Earth & Environment*, *3*(1), 288. doi: 10.1038/s43247-022-00618-z

Tabazadeh, A., Toon, O. B., Clegg, S. L., & Hamill, P. (1997). A new parameterization of H2SO4/H2O aerosol composition: Atmospheric implications. *Geophysical Research Letters*, *24*(15), 1931-1934. doi: 10.1029/97GL01879

Taha, G., Loughman, R., Colarco, P. R., Zhu, T., Thomason, L. W., & Jaross, G. (2022). Tracking the 2022 Hunga Tonga-Hunga Ha'apai Aerosol Cloud in the Upper and Middle Stratosphere Using Space-Based Observations. *Geophysical Research Letters*, *49*(19), e2022GL100091. doi: 10.1029/2022GL100091

von Savigny, C., & Hoffmann, C. G. (2020). Issues related to the retrieval of stratospheric-aerosol particle size information based on optical measurements. *Atmospheric Measurement Techniques*, *13*(4), 1909–1920. doi: 10.5194/amt-13-1909-2020

Wiscombe, W. J. (1979). *Mie scattering calculations: Advances in technique and fast, vector-speed computer codes* (Vol. 10). National Technical Information Service, US Department of Commerce.

Wrana, F., Niemeier, U., Thomason, L. W., Wallis, S., & von Savigny, C. (2023). Stratospheric aerosol size reduction after volcanic eruptions. *preprint*, *2023*, 1–30. doi: 10.5194/egusphere-2023-837

Wrana, F., von Savigny, C., Zalach, J., & Thomason, L. W. (2021). Retrieval of stratospheric aerosol size distribution parameters using satellite solar occultation measurements at three wavelengths. *Atmospheric Measurement Techniques*, *14*(3), 2345–2357. doi: 10.5194/amt-14-2345-2021

Zhang, H., Wang, F., Li, J., Duan, Y., Zhu, C., & He, J. (2022). Potential Impact of Tonga Volcano Eruption on Global Mean Surface Air Temperature. *Journal of Meteorological Research*, *36*(1), 1–5. doi: 10.1007/s13351-022-2013-6

Zhu, Y., Bardeen, C. G., Tilmes, S., Mills, M. J., Wang, X., Harvey, V. L., ... Toon, O. B. (2022). Perturbations in stratospheric aerosol evolution due to the water-rich plume of the 2022 Hunga-Tonga eruption. *Communications Earth & Environment*, *3*(1), 248. doi: 10.1038/s43247-022-00580-w

Observation of the aerosol plume from the 2022 Hunga Tonga – Hunga Ha'apai eruption with SAGE III/ISS

Clair Duchamp[1], Felix Wrana[2], Bernard Legras[1], Pasquale Sellitto[3,4], Redha Belhadji[3], Christian von Savigny[2]

[1]Laboratoire de Météorologie Dynamique (LMD-IPSL), CNRS, Sorbonne Université, ENS-PSL, École Polytechnique, Paris, France
[2]Institute of Physics, University of Greifswald, Greifswald, Germany
[3]Univ. Paris Est Créteil and Université de Paris-Cité, CNRS, Laboratoire Interuniversitaire des Systèmes Atmosphériques (LISA-IPSL), Créteil, France
[4]Istituto Nazionale di Geofisica e Vulcanologia (INGV), Osservatorio Etneo (OE), Catania, Italy

Key Points:

- The extinction of the stratospheric plume of the 2022 Tonga eruption is well modeled by a unimodal distribution of sulfate particles.
- The effective radius of the aerosols is large with values close to 0.4 µm, and a mode width of 1.25, from March 2022 to April 2023.
- We estimate a total H_2SO_4 mass in stratospheric sulfate aerosols of about 0.66 Tg corresponding to 0.44 Tg of SO_2 at the source.

Corresponding author: Clair Duchamp, clair.duchamp@lmd.ipsl.fr

Abstract

The Tonga eruption of 15 January 2022 has released a long-lived stratospheric plume of sulfate aerosols. More than 15 months after, we focus on the high quality data series of SAGE III/ISS to determine the mean radius and size distribution of the aerosols and their total mass. We show that the peristing aerosols – with a mode width of 1.25 and an effective radius of 0.4 µm – differ from the significantly smaller background aerosols and from those measured during other recent stratospheric eruptions. The sulfuric acid mass between 50°S and 30°N is estimated to be very stable in spite of considerable redistribution in latitude at a value of 0.66 Tg ± 0.1 Tg, corresponding to an initial sulfur dioxide emission of 0.44 Tg. Such properties are expected to induce a small negative aerosol radiative forcing, thus facilitating the persistence of a climate warming due to the volcanic water vapour.

Plain Language Summary

We study the stratospheric aerosol plume produced by the Hunga Tonga–Hunga Ha'apai eruption on 15 January 2022 based on the high quality solar occultation measurements of the instrument SAGE III onboard the ISS. These data reveal that the aerosol sizes are about twice as large as after other documented volcanic eruptions and that the total mass of H_2SO_4 in the liquid droplets of sulfate in the stratosphere has been very stable from March 2022, when it started to be well homogeneized in longitude, to November 2022, when it started to decay. The total mass of 0.66 Tg of H_2SO_4 is in good agreement with the early estimates of a stratospheric emission of 0.4-0.5 Tg of SO_2. The implication is that the aerosol radiative impact will not mask the persisting warming effect of the water vapour injected in the stratosphere by the eruption.

1 Introduction

The phreato-magmatic eruption of the Hunga Tonga-Hunga Ha'apai (HTHH) started on 20 December 2021 and went through an explosive phase on 15 January 2022 which was comparable in Volcanic Explosivity Index with Pinatubo (Poli & Shapiro, 2022). The atmospheric plume was exceptional by reaching the mesosphere with a maximum height of 58 km and by injecting a considerable amount of water that saturated the stratosphere at least up to 35 km leaving a +10% increase of the stratospheric water vapour (Carr et al., 2022; Millán et al., 2022; Khaykin et al., 2022). The initial injection of water might have been much larger as the estimated amount of solid ejecta is close to 7 km^3 (O'Callaghan, 2022) but the water in excess above saturation condensed rapidly and precipitated entraining the ash that mostly disappeared from the stratosphere (Legras et al., 2022). As a matter of fact, besides a thin cloud detected at 35 km during a few days (Khaykin et al., 2022; Baron et al., 2023), no depolarizing aerosols have been detected in the stratosphere above 18 km in the aftermath of the eruption (Legras et al., 2022), indicating that ash did not play an important role. In contrast to water, the early estimates of the SO_2 injection at 0.4-0.5 Tg (Millán et al., 2022; Carn et al., 2022) were modest compared to the 20 Tg of Pinatubo (Guo et al., 2004) and even to the 1.5 Tg of Raikoke (de Leeuw et al., 2021). However, the moist environment induced a fast conversion to sulfate aerosols (SA) (Zhu et al., 2022) that were detected as non depolarizing, presumably spherical, particles and the conversion was basically complete by the end of January (Legras et al., 2022). It was suggested that the initial estimate could have missed a large amount of already converted SO_2 and estimates of up to 1.5 Tg have been speculated on (Sellitto et al., 2022; Legras et al., 2022). Several estimates of the average size of the aerosols and of their evolution ranging from 0.2 µm to 1 µm have been provided from satellite retrievals and in situ measurements (Kloss et al., 2022; Schoeberl et al., 2022; Taha et al., 2022; Legras et al., 2022; Khaykin et al., 2022; Baron et al., 2023). Such dispersion has considerable impact on the persistence of aerosols in the stratosphere and their radiative im-

pact (Zhu et al., 2022; Sellitto et al., 2022; Zhang et al., 2022). More than 15 months after the eruption, the goal of this work is to provide a well documented survey of the size and distribution of the aerosols, using minimal assumptions by taking advantage of the high quality measurements of SAGE III/ISS.

2 Data & Methods

2.1 SAGE III/ISS

The instrument Stratospheric Aerosol and Gas Experiment III (SAGE III), onboard the International Space Station (ISS), has been providing measurements of solar and lunar occultation since June 2017 (Cisewski et al., 2014). The instrument provides aerosol extinctions at 9 wavelengths from 384 nm to 1543 nm, the latter near-infrared channel being an addition with respect to SAGE II which significantly extends the spectral range. The data are provided in 0.5 km steps between 0 and 45 km altitude. The instrument observes about 15 sunrises and 15 sunsets per day with a latitudinal range which varies depending on the period of year (cf Table S1). In particular, there are no profiles at higher latitudes than 50°S between May and July 2022. The aerosol extinctions are retrieved as residuals of a spectral multilinear fit for O_3 and N_2O but do not require any size distribution assumptions unlike instruments with limb-scatter geometry like OMPS-LP (Loughman et al., 2018).

For this study, we use the version 5.3 of the SAGE III/ISS level 2 solar aerosol product. The profiles are monthly averaged in four latitude bands of width $\Delta\phi = 20°$, using data from November 2021 to April 2023. Due to its sparse geographical sampling, SAGE III began to see the HTHH SA plume only in March 2022 limiting our approach to the months after March 2022. During January and February 2022, SAGE III seldom sampled the plume and data are used for comparison between the plume and background conditions.

2.2 Retrieval of aerosol size parameters at 3 wavelengths

We use a method implemented by Wrana et al. (2021) to retrieve the SA size distribution which is based on the two color ratios 449 nm / 755 nm and 1543 nm / 755 nm for the aerosol extinction coefficients. These ratios are modeled for spherical liquid SA through Mie calculations using miepython, a python code where the Mie theory is implemented following the procedure described by Wiscombe (1979). We use fixed refractive indices from the GEISA spectroscopic database (Armante et al., 2016), for a temperature of 215 K and a H_2SO_4 weight proportion w_s of 70 % considering that the rest of the liquid droplet is water (Biermann et al., 2000). This weight proportion has been obtained according to Tabazadeh et al. (1997) using ambient temperature and moisture of the plume. As the SA have a very low absorption in the short wave spectral range (Palmer & Williams, 1975), we fix the imaginary part of the refractive index to 10^{-6}. Due to the presumed absence of ash, we assume that the particle size distribution (PSD) follows a monomodal lognormal distribution law.

$$\mathcal{N} = \frac{N_0}{\sqrt{2\pi} r \ln \sigma} \exp\left(-\frac{\ln^2 (r/r_m)}{2 \ln^2 \sigma}\right) \tag{1}$$

where σ is the mode width, r_m is the median radius and N_0 is the number density. The aerosol extinction k_{ext} at wavelength λ is then obtained by an integration over the size distribution

$$k_{ext}(\lambda) = \int_0^{+\infty} Q_{ext}(r, n, \lambda) \cdot \pi r^2 \cdot \mathcal{N}(r, r_m, \sigma, N_0)\, \mathrm{d}r \tag{2}$$

where Q_{ext} is the extinction efficiency factor from Mie calculations and n is the refractive index.

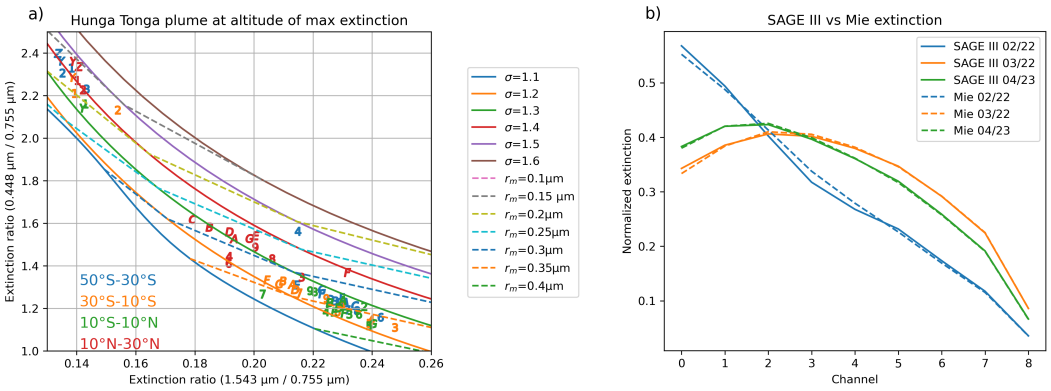

Figure 1. (a) The solid curves correspond to Mie calculations of the extinction ratios 448 nm / 755 nm and 1543 nm / 755 nm for constant values of the width σ. The dashed curves correspond to constant values of the mean radius r_m. This figure uses the same axis as Fig. 2a of Wrana et al. (2021). The numbers and letters show SAGE III measured ratios for each latitude band (color coded) and month at the central level of maximum 755 nm extinction for each month. The months are coded as Y and Z for November and December 2021, as 1 to 9 between January and September 2022 and alphabetically from A to G between October 2022 and April 2023. For each latitude band, the altitude levels for months before February 2022 (and March for the 40°S band) are chosen to be the same as the central level for the first detection in March 2022 (or April for the 40°S band). (b) Comparison of SAGE III (solid) and modeled (dash) normalized extinctions for all 9 aerosol channels of SAGE III. The curves are shown for the latitude band 30°S - 10°S using the values of σ and r_m determined from the diagram (a). We show the background case of February 2022 (blue) and the earliest and latest case of the plume in March 2022 (orange) and April 2023 (green).

In the estimation of the two extinction ratios mentioned above, the N_0 parameter cancels out, and we are left with a dependency on σ and r_m only. Fig. 1a shows that the curves for equal σ and r_m form a skewed grid in the domain of interest allowing the identification of the two parameters. The separation of spectral channels in terms of wavelengths in the two ratios is critical to obtain such results as shown by Wrana et al. (2021). For each data point from SAGE III extinctions the corresponding σ and r_m values are obtained by interpolating linearly between the discretized curves shown in Fig. 1a. Then, the particle effective radius r_{eff} can be estimated as $r_{eff} = r_m \exp\left(\frac{5}{2}\ln^2\sigma\right)$. Finally, we can compute the total number density N_0 from Eq. (2) using the extinction at 755 nm.

The good performance of the method can be appreciated from Fig. 1b where modeled Mie extinctions using σ and r_m drawn from Fig. 1a are compared to the SAGE III measured extinctions for three cases, one in the background and two in the plume at one-year distance. We see that the agreement is excellent over the whole range in spite of the obvious differences between the background and the plume cases. This is consistent with the absence of a coarser mode due to ash but does not rule out the presence of a finer mode which cannot be distinguished by extinction measurements (von Savigny & Hoffmann, 2020). The fact that estimates of sizes from fall speed (Schoeberl et al., 2022; Legras et al., 2022; Khaykin et al., 2022) using measurements by limb scatter or lidar backscatter are of the order or larger than our own estimate is an indication that such a fine mode is not important here as the lidar measurements in particular would be much more sensitive to it than solar occultation measurements (von Savigny & Hoffmann, 2020).

2.3 Estimation of the H_2SO_4 total mass

The H_2SO_4 mass is estimated for each vertical layer and latitude band from the estimated values of σ and r_m in this domain. The volume proportion of H_2SO_4 in a droplet is $\gamma(w_s) = (1 + \frac{\rho_s}{\rho_w}(\frac{1}{w_s} - 1))^{-1}$ where ρ_s is the density of pure H_2SO_4 and ρ_w is the water density, and the H_2SO_4 mass of the droplet is $m_p(r, w_s) = \frac{4}{3}\pi r^3 \gamma(w_s)\rho_s$.

Integrating over the lognormal distribution, we find that the H_2SO_4 mass contained in a layer centered at latitude ϕ is :

$$m_l = V_l(\phi) \cdot m_p(r_m, w_s) \cdot \alpha(\sigma) \cdot N_0 \tag{3}$$

where $\alpha(\sigma) = \exp(\frac{9}{2}\ln^2\sigma)$ is the lognormal volume ratio and $V_l(\phi) = 4\pi R^2 H \cos\phi \sin(\Delta\phi/2)$ is the volume of the layer with $R = 6371$ km and $H = 500$ m.

Summing m_l over all the layers of the plume, we calculate the total mass for each month and each latitude band for a given w_s. Unless otherwise specified, we use $w_s =$ 70 %.

3 Results

The first row of Fig. 2 shows that the aerosol plume has persisted as a distinguished layer in the stratosphere until April 2023, 15 months after the eruption. Until May 2022 the plume was mainly contained between 30°S and 10°N and then started to spread towards higher latitudes in the southern hemisphere. In spite of the detection of filaments at high latitudes (Mishra et al., 2022; Khaykin et al., 2022), there was little spread beyond the equatorial band in the northern hemisphere. The plume descended constantly until November 2022 but with a latitude dependent speed, in agreement with the Brewer-Dobson circulation, the descent being faster at high latitudes. Since November 2022, the maximum extinction altitude has been stalling at mid-latitudes and slightly rising in the equatorial band. It is noticeable that for all latitudes north of 30°S the aerosol layer does not disperse in altitude and keeps a fairly constant thickness.

In Fig. 1a, the observed extinction ratios at the level of maximum extinction in the plume are distributed over a domain of the diagram that clearly differs from the back-

ground points. These latter match the values reported in Wrana et al. (2021) with width σ of 1.4-1.5 and radius r_m of 0.15-0.2 µm. Instead, all the plume points south of 10°N but a couple of outliers lay between the 1.2 and 1.3 σ curves and cluster around $r_m \approx 0.35$ µm. This finding of low σ values is important, since usually very different assumptions are made, e.g. in satellite limb-scatter retrievals or in size retrievals using a 2 wavelength-extinction-ratio approach, which can introduce strong retrieval biases. The part of the plume in the 10°N - 30°N range forms a separate cluster with smaller radius between 0.25 and 0.30 µm and $\sigma \approx 1.3$. April 2022 for the 40°S latitude band is a mixed case between background and plume conditions when aerosols begin to reach these latitudes (as seen on Fig. 2, first row). Fig. S1 shows that retrieval uncertainties do not jeopardize the separation between the background and the plume. It also shows that at all latitudes the mean size decreases with time albeit by a small amount but no trend can be detected for the width. From σ and r_m, we calculate r_{eff} which is near 0.4 µm in the plume while we find 0.2 µm or less for the background in agreement with Khaykin et al. (2022).

The full temporal evolution of σ and r_{eff} is shown in the second and third rows of Fig. 2. The homogeneity and the persistence of the properties across the plume and in time are clearly visible. Using the same method, Wrana et al. (2023) found σ values for other stratospheric volcanic plumes produced by the eruptions of Ambae in 2018, Raikoke and Ulawun in 2019 and La Soufrière in 2021, which are all larger, approaching respectively 1.5-1.6 and 1.8-2.0 (Wrana et al., 2023), reinforcing the exceptional aspect of the HTHH eruption.

The total number density N_0 is shown in the last row of Fig. 2. The largest values of about 5 cm^{-3} are found in the early stage of the equatorial band. Values of 3.5 cm^{-3} are maintained until September 2022 and are slowly declining afterwards.

Fig. 3 shows 2 retrieved PSD in the same latitude band and altitude range for the background conditions and the plume. We stress that the HTHH eruption actually led to a much wider size distribution than in the background, even though the mode width σ is strongly reduced. This is because σ is the distribution width in logarithmic radius space, not linear radius space.

Fig. 4a shows the total amount of H_2SO_4 mass in the plume SA and the background mass contribution in the volume of the plume, according to Eq. (3) for a value of the mass proportion w_s of 70%. The total amount between 50°S and 30°N remains remarkably constant from March 2022 to November 2022 in spite of a considerable redistribution in latitude which is shown in Fig. 4b. The fast transport to the equatorial band during the first month following the eruption mentioned by Schoeberl et al. (2023) generates an equatorial dominance until May 2022 which is followed by a transport to the 40°S band which dominates from August to November 2022. The total mass decline after November 2022 is mainly due to this latitude band, presumably because of the sedimentation towards the lowest stratosphere and return to the troposphere. The equatorial band and the 20°S band essentially exchange aerosol mass while maintaining a constant sum from August 2022 onward. Taking into account the high latitude contribution in the southern hemisphere, which can only be estimated from October 2022, adds 0.1 Tg to the total but does not contribute to the decline. If a distribution of sulfate representing a background component (to be substracted) is taken into account within the volume of the plume (see Fig. 4a), this represents a small correction which increases with the volume of the plume but is always less than 0.1 Tg. Accounting these errors, we estimate the total mass of H_2SO_4 between March and November 2022 to be 0.66 Tg ± 0.1 Tg for $w_s = 70\%$. It scales proportionally to w_s if another value is assumed.

Converting the H_2SO_4 total mass into a SO_2 source using the molar mass ratio produces an estimate of 0.44 Tg of SO_2 for 0.66 Tg of H_2SO_4 which is in good agreement with the early estimates (Millán et al., 2022; Carn et al., 2022) produced from satellite observations.

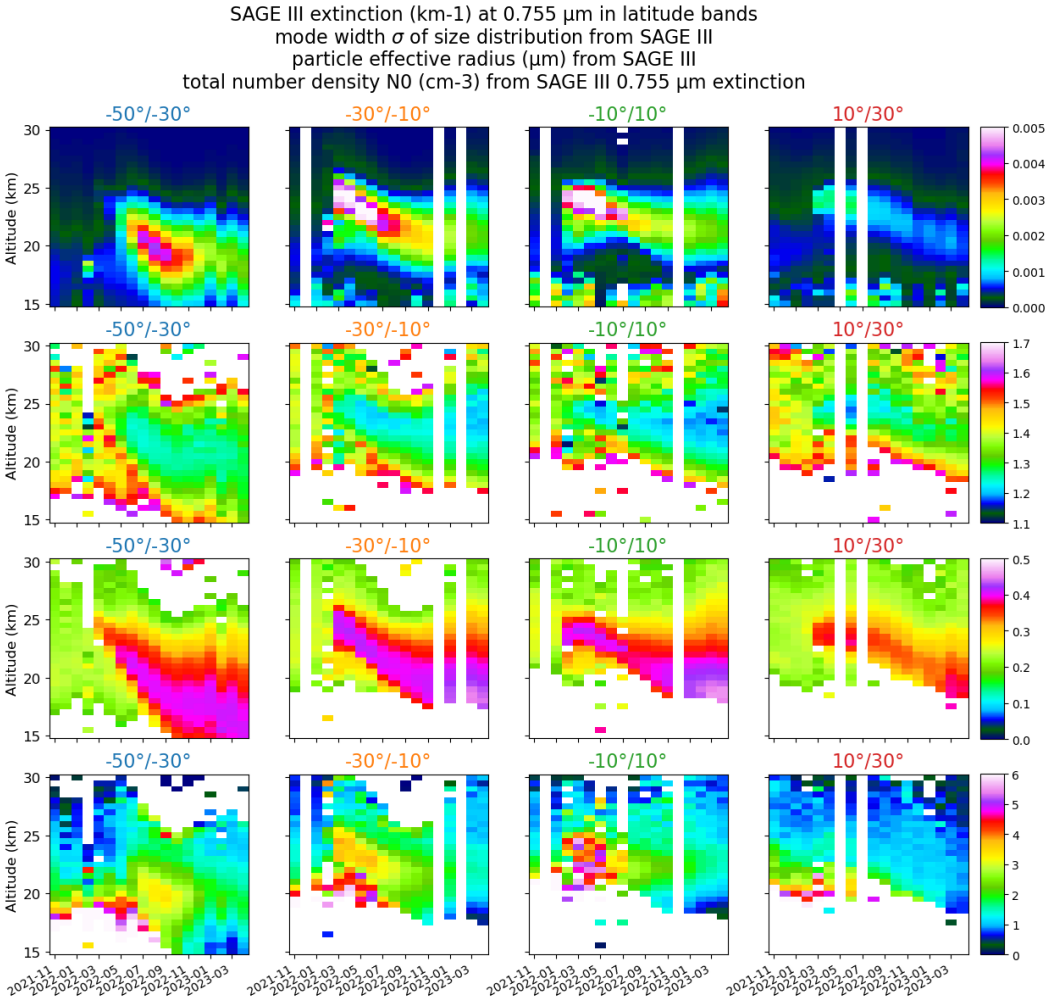

Figure 2. Zonal altitude-time sections averaged over 20° latitude bands between 50°S and 30°N. The first row represents the aerosol extinction k_{ext} (km^{-1}) provided by SAGE III at 755 nm. The second row represents the mode width σ of the PSD retrieved from SAGE III extinction ratios. The third row represents the particle effective radius r_{eff} (µm). The fourth row represents the total number density N_0 (cm^{-3}) of the PSD retrieved from SAGE III extinction ratios and 755 nm extinction k_{ext}.

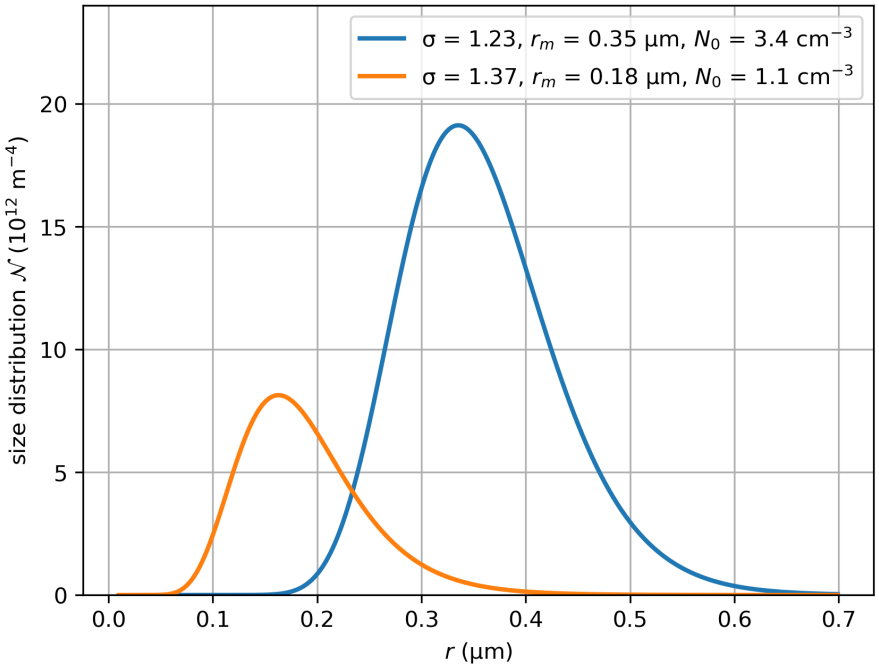

Figure 3. Monthly averaged particle size distributions from the retrieved PSD parameters in the 30°S - 10°S latitude range. Orange curve corresponds to background conditions at 24.5 km averaged between months of November 2021 and January 2022, blue curve corresponds to plume conditions at altitude of maximum extinction averaged between months of June and August 2022.

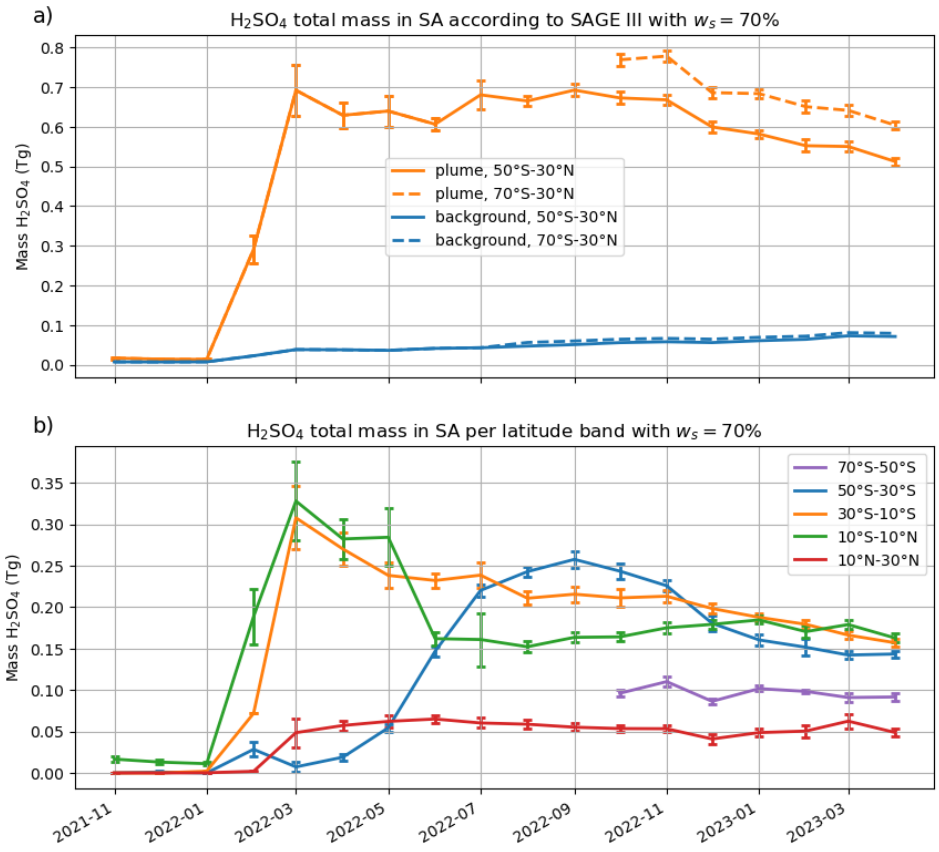

Figure 4. (a) Orange curves: evolution of the H_2SO_4 total mass contained in the plume sulfates for a H_2SO_4 weight percentage $w_s = 70\%$, according to SAGE III, eliminating surrounding pixels with radius r_m less than 0.2 µm considered as background. Blue curves: background contribution within the volume of the plume with $\sigma = 1.4$, $r_m = 0.15$ µm and $N_0 = 1$ cm^{-3}. The latitude range is 50°S - 30°N for solid curves and 70°S - 30°N for dashed curves. (b) Evolution of the H_2SO_4 total mass per latitude band. The contribution from the 50°S - 70°S is zero before May 2022, then is missing until August and contaminated by polar stratospheric clouds until September. It is shown only from October.

4 Conclusions

The HTHH eruption led to a large perturbation in stratospheric aerosols still visible 15 months after the eruption in solar occultation measurements of the satellite instrument SAGE III/ISS. The comparison of these measurements with theoretical Mie calculations supports the hypothesis of the absence of any optical signature of ash. Assuming a monomodal size distribution of liquid spherical sulfate aerosols, we estimate the mode width and the effective radius to the unusual values of $\sigma \approx 1.25$ and $r_{eff} \approx 0.4\,\mu m$ which have persisted at the plume peak height over 15 months with only a small decreasing trend in the size. The additional estimate of the total number density leads to an estimate of the total mass of stratospheric H_2SO_4 which is near 0.66 Tg for a mass proportion of 70% and has been found to be very stable over the period March 2022 to November 2022 after which it slowly declines. This mass matches very well previous estimates of the stratospheric SO_2 source of about 0.4-0.5 Tg (Millán et al., 2022; Carn et al., 2022).

The unusual size distribution of aerosols is related to the fast conversion of SO_2 to sulfates and possible sustained condensation/coagulation under very moist conditions documented by, e.g., Legras et al. (2022) and modeled by Zhu et al. (2022). Larger particles than recent stratospheric volcanic eruptions, like Raikoke and others, can be associated with a smaller aerosol radiative impact (Lacis et al., 1992). In the case of the extremely water-vapor-rich Hunga Tonga plume, this, in turns, facilitate the persistence of a global warming volcanic plume, as discussed by Sellitto et al. (2022).

Open Research Section

SAGE III/ISS L2 Solar Event Species Profiles (HDF5) V053 dataset is available from `https://doi.org/10.5067/ISS/SAGEIII/SOLAR_NetCDF4_L2-V5.3`. miepython is a free package available from `https://miepython.readthedocs.io/en/latest/` and `https://doi.org/10.5281/zenodo.8023972`. We used version 2.3.0 in this study. AERIS has provided access to the GEISA database at `https://geisa.aeris-data.fr`.

Acknowledgments

This study has been supported by the Agence Nationale de la Recherche under grant 21-CE01-0007-01 (ANR ASTuS) and the Centre National d'Études Spatiales (CNES). Work at the University of Greifswald was funded by the Deutsche Forschungsgemeinschaft (DFG Research Unit VolImpact, grant number 398006378).

References

Armante, R., Scott, N., Crevoisier, C., Capelle, V., Crepeau, L., Jacquinet, N., & Chédin, A. (2016, September). Evaluation of spectroscopic databases through radiative transfer simulations compared to observations. Application to the validation of GEISA 2015 with IASI and TCCON. *Journal of Molecular Spectroscopy*, *327*, 180–192. doi: 10.1016/j.jms.2016.04.004

Baron, A., Chazette, P., Khaykin, S., Payen, G., Marquestaut, N., Bègue, N., & Duflot, V. (2023). Early Evolution of the Stratospheric Aerosol Plume Following the 2022 Hunga Tonga-Hunga Ha'apai Eruption: Lidar Observations From Reunion (21°S, 55°E). *Geophysical Research Letters*, *50*(10), e2022GL101751. doi: /10.1029/2022GL101751

Biermann, U. M., Luo, B. P., & Peter, T. (2000). Absorption Spectra and Optical Constants of Binary and Ternary Solutions of H2SO4, HNO3, and H2O in the Mid Infrared at Atmospheric Temperatures. *The Journal of Physical Chemistry A*, *104*(4), 783-793. doi: 10.1021/jp992349i

Carn, S. A., Krotkov, N. A., Fisher, B. L., & Li, C. (2022). Out of the blue: Vol-

canic SO2 emissions during the 2021–2022 eruptions of Hunga Tonga—Hunga Ha'apai (Tonga). *Frontiers in Earth Science*, *10*, 976962. doi: 10.3389/feart.2022.976962

Carr, J. L., Horvath, A., Wu, D. L., & Friberg, M. D. (2022). Stereo Plume Height and Motion Retrievals for the Record-Setting Hunga Tonga-Hunga Ha'apai Eruption of 15 January 2022. *Geophysical Research Letters*, *49*, e2022GL098131. doi: 10.1029/2022GL098131

Cisewski, M., Zawodny, J., Gasbarre, J., Eckman, R., Topiwala, N., Rodriguez-Alvarez, O., ... Hall, S. (2014). The Stratospheric Aerosol and Gas Experiment (SAGE III) on the International Space Station (ISS) Mission. In R. Meynart, S. P. Neeck, & H. Shimoda (Eds.), *Sensors, systems, and next-generation satellites xviii* (Vol. 9241, p. 924107). SPIE. doi: 10.1117/12.2073131

de Leeuw, J., Schmidt, A., Witham, C. S., Theys, N., Taylor, I. A., Grainger, R. G., ... Kristiansen, N. I. (2021). The 2019 Raikoke volcanic eruption – Part 1: Dispersion model simulations and satellite retrievals of volcanic sulfur dioxide. *Atmospheric Chemistry and Physics*, *21*(14), 10851–10879. doi: 10.5194/acp-21-10851-2021

Guo, S., Bluth, G. J. S., Rose, W. I., Watson, I. M., & Prata, A. J. (2004). Re-evaluation of SO2 release of the 15 June 1991 Pinatubo eruption using ultraviolet and infrared satellite sensors. *Geochemistry, Geophysics, Geosystems*, *5*(4). doi: 10.1029/2003GC000654

Khaykin, S., Podglajen, A., Ploeger, F., Grooß, J.-U., Tence, F., Bekki, S., ... Ravetta, F. (2022). Global perturbation of stratospheric water and aerosol burden by Hunga eruption. *Communications Earth & Environment*, *3*(1), 316. doi: 10.1038/s43247-022-00652-x

Kloss, C., Sellitto, P., Renard, J.-B., Baron, A., Bègue, N., Legras, B., ... Jégou, F. (2022). Aerosol Characterization of the Stratospheric Plume From the Volcanic Eruption at Hunga Tonga 15 January 2022. *Geophysical Research Letters*, *49*(16), e2022GL099394. doi: 10.1029/2022GL099394

Lacis, A., Hansen, J., & Sato, M. (1992). Climate forcing by stratospheric aerosols. *Geophysical Research Letters*, *19*(15), 1607-1610. doi: 10.1029/92GL01620

Legras, B., Duchamp, C., Sellitto, P., Podglajen, A., Carboni, E., Siddans, R., ... Ploeger, F. (2022). The evolution and dynamics of the Hunga Tonga–Hunga Ha'apai sulfate aerosol plume in the stratosphere. *Atmospheric Chemistry and Physics*, *22*(22), 14957–14970. doi: 10.5194/acp-22-14957-2022

Loughman, R., Bhartia, P. K., Chen, Z., Xu, P., Nyaku, E., & Taha, G. (2018). The Ozone Mapping and Profiler Suite (OMPS) Limb Profiler (LP) Version 1 aerosol extinction retrieval algorithm: theoretical basis. *Atmospheric Measurement Techniques*, *11*(5), 2633–2651. doi: 10.5194/amt-11-2633-2018

Millán, L., Santee, M. L., Lambert, A., Livesey, N. J., Werner, F., Schwartz, M. J., ... Froidevaux, L. (2022). The Hunga Tonga-Hunga Ha'apai Hydration of the Stratosphere. *Geophysical Research Letters*, *49*(13), e2022GL099381. doi: 10.1029/2022GL099381

Mishra, M. K., Hoffmann, L., & Thapliyal, P. K. (2022). Investigations on the Global Spread of the Hunga Tonga-Hunga Ha'apai Volcanic Eruption Using Space-Based Observations and Lagrangian Transport Simulations. *Atmosphere*, *13*(12), 2055. doi: 10.3390/atmos13122055

O'Callaghan, J. (2022). Burst of underwater explosions powered Tonga volcano eruption. *Nature*, d41586–022–01544–y. doi: 10.1038/d41586-022-01544-y

Palmer, K. F., & Williams, D. (1975). Optical constants of sulfuric acid; application to the clouds of Venus? *Applied Optics*, *14*(1), 208–219. doi: 10.1364/AO.14.000208

Poli, P., & Shapiro, N. M. (2022). Rapid Characterization of Large Volcanic Eruptions: Measuring the Impulse of the Hunga Tonga Ha'apai Explosion From Teleseismic Waves. *Geophysical Research Letters*, *49*(8), e2022GL098123. doi:

10.1029/2022GL098123

Schoeberl, M. R., Wang, Y., Ueyama, R., Taha, G., Jensen, E., & Yu, W. (2022). Analysis and Impact of the Hunga Tonga-Hunga Ha'apai Stratospheric Water Vapor Plume. *Geophysical Research Letters*, *49*(20), e2022GL100248. doi: doi.org/10.1029/2022GL100248

Schoeberl, M. R., Wang, Y., Ueyama, R., Taha, G., & Yu, W. (2023). The Cross Equatorial Transport of the Hunga Tonga-Hunga Ha'apai Eruption Plume. *Geophysical Research Letters*, *50*(4), e2022GL102443. doi: 10.1029/2022GL102443

Sellitto, P., Podglajen, A., Belhadji, R., Boichu, M., Carboni, E., Cuesta, J., ... Legras, B. (2022). The unexpected radiative impact of the Hunga Tonga eruption of 15th January 2022. *Communications Earth & Environment*, *3*(1), 288. doi: 10.1038/s43247-022-00618-z

Tabazadeh, A., Toon, O. B., Clegg, S. L., & Hamill, P. (1997). A new parameterization of H2SO4/H2O aerosol composition: Atmospheric implications. *Geophysical Research Letters*, *24*(15), 1931-1934. doi: 10.1029/97GL01879

Taha, G., Loughman, R., Colarco, P. R., Zhu, T., Thomason, L. W., & Jaross, G. (2022). Tracking the 2022 Hunga Tonga-Hunga Ha'apai Aerosol Cloud in the Upper and Middle Stratosphere Using Space-Based Observations. *Geophysical Research Letters*, *49*(19), e2022GL100091. doi: 10.1029/2022GL100091

von Savigny, C., & Hoffmann, C. G. (2020). Issues related to the retrieval of stratospheric-aerosol particle size information based on optical measurements. *Atmospheric Measurement Techniques*, *13*(4), 1909–1920. doi: 10.5194/amt-13-1909-2020

Wiscombe, W. J. (1979). *Mie scattering calculations: Advances in technique and fast, vector-speed computer codes* (Vol. 10). National Technical Information Service, US Department of Commerce.

Wrana, F., Niemeier, U., Thomason, L. W., Wallis, S., & von Savigny, C. (2023). Stratospheric aerosol size reduction after volcanic eruptions. *preprint*, *2023*, 1–30. doi: 10.5194/egusphere-2023-837

Wrana, F., von Savigny, C., Zalach, J., & Thomason, L. W. (2021). Retrieval of stratospheric aerosol size distribution parameters using satellite solar occultation measurements at three wavelengths. *Atmospheric Measurement Techniques*, *14*(3), 2345–2357. doi: 10.5194/amt-14-2345-2021

Zhang, H., Wang, F., Li, J., Duan, Y., Zhu, C., & He, J. (2022). Potential Impact of Tonga Volcano Eruption on Global Mean Surface Air Temperature. *Journal of Meteorological Research*, *36*(1), 1–5. doi: 10.1007/s13351-022-2013-6

Zhu, Y., Bardeen, C. G., Tilmes, S., Mills, M. J., Wang, X., Harvey, V. L., ... Toon, O. B. (2022). Perturbations in stratospheric aerosol evolution due to the water-rich plume of the 2022 Hunga-Tonga eruption. *Communications Earth & Environment*, *3*(1), 248. doi: 10.1038/s43247-022-00580-w

Supplement to "Observation of the aerosol plume from the 2022 Hunga Tonga – Hunga Ha'apai eruption with SAGE III/ISS"

Clair Duchamp[1], Felix Wrana[2], Bernard Legras[1], Pasquale Sellitto[3,4], Redha Belhadji[3], Christian von Savigny[2]

[1]Laboratoire de Météorologie Dynamique (LMD-IPSL), CNRS, Sorbonne Université, ENS-PSL, École Polytechnique, Paris, France
[2]Institute of Physics, University of Greifswald, Greifswald, Germany
[3]Univ. Paris Est Créteil and Université de Paris-Cité, CNRS, Laboratoire Interuniversitaire des Systèmes Atmosphériques (LISA-IPSL), Créteil, France
[4]Istituto Nazionale di Geofisica e Vulcanologia (INGV), Osservatorio Etneo (OE), Catania, Italy

S1 Number of SAGE III profiles

Table S1. Number of vertical profiles of SAGE III per latitude band and month.

	70°S-50°S	50°S-30°S	30°S-10°S	10°S-10°N	10°N-30°N
02/2022	317	4	1	44	85
03/2022	32	186	69	70	43
04/2022	93	309	102	88	113
05/2022	0	217	71	5	0
06/2022	0	287	134	113	110
07/2022	0	218	82	1	0
08/2022	45	340	119	99	118
09/2022	56	120	99	69	60
10/2022	393	91	55	61	92
11/2022	59	145	112	45	77
12/2022	263	49	0	0	63
01/2023	94	127	124	93	100
02/2023	237	24	0	40	53
03/2023	48	160	76	72	42
04/2023	77	328	93	91	112

S2 Evolution of σ and r_m

Corresponding author: Clair Duchamp, clair.duchamp@lmd.ipsl.fr

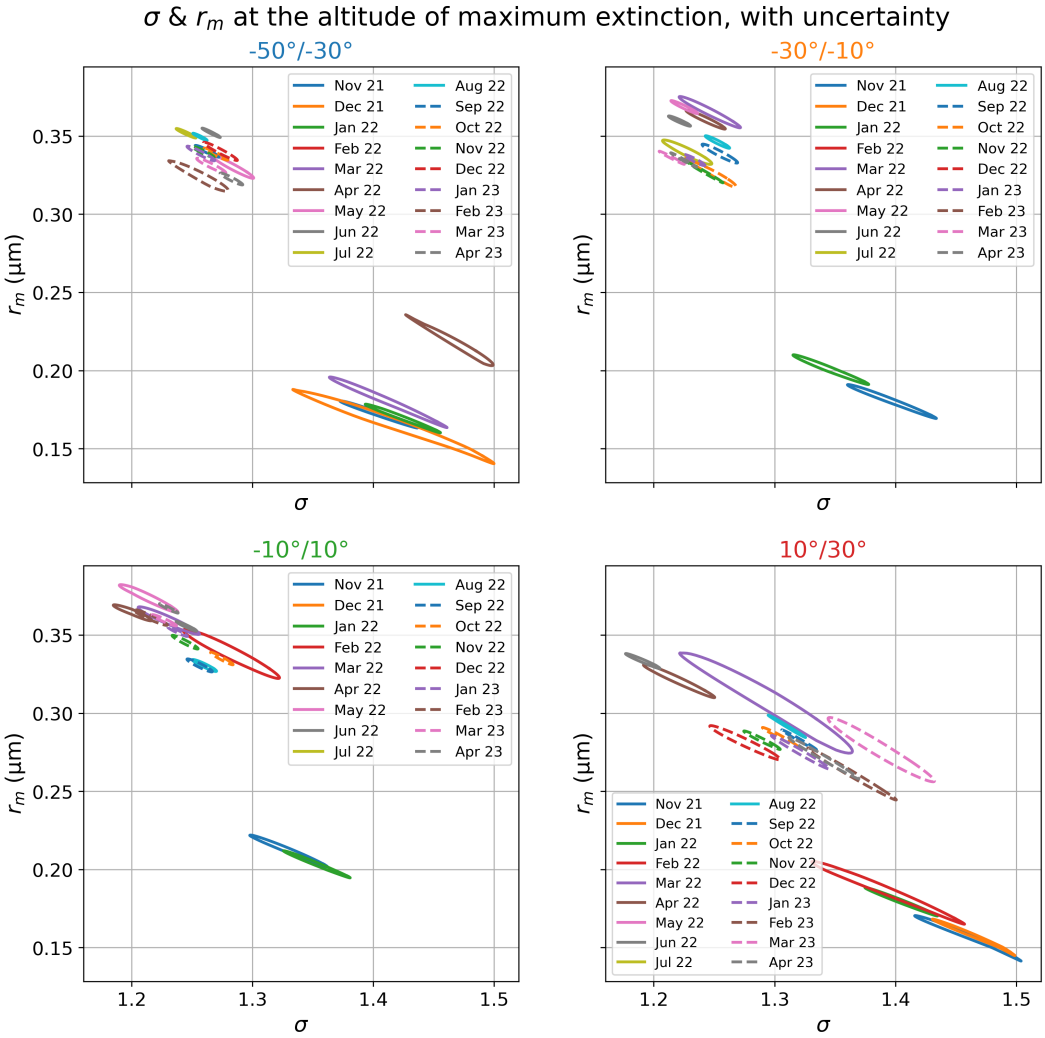

Figure S1. Estimates of σ and r_m at the altitude of the maximum extintion as a function of time. For each month, the uncertainty in σ and r_m is drawn from the ellipse representing the uncertainty in the two extinction ratios in the plane of Fig. 1b.